NASA TN D-119

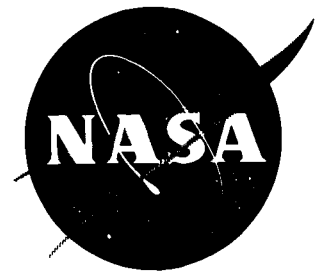

TECHNICAL NOTE
D-119

INVESTIGATION OF A HIGH-SPEED HYDROFOIL WITH PARABOLIC THICKNESS DISTRIBUTION

By Virgil E. Johnson, Jr., and Thomas A. Rasnick

Langley Research Center
Langley Field, Va.

NATIONAL AERONAUTICS AND SPACE ADMINISTRATION

WASHINGTON

November 1959

NATIONAL AERONAUTICS AND SPACE ADMINISTRATION

TECHNICAL NOTE D-119

INVESTIGATION OF A HIGH-SPEED HYDROFOIL WITH PARABOLIC THICKNESS DISTRIBUTION

By Virgil E. Johnson, Jr., and Thomas A. Rasnick

SUMMARY

Principles of both fully wetted and supercavitating flow theory are utilized to design a thick hydrofoil with acceptable hydrodynamic efficiency in the 100-knot (169 fps) speed range. The hydrofoil design incorporates mean-line camber with a parabolic thickness distribution. A model of the cambered parabolic section with an aspect ratio of 1 and a base thickness of 0.1 chord was investigated at a depth of 0.5 chord for a range of angles of attack from 1° to 8° and speeds from 130 to 190 feet per second. The results of the investigation showed maximum lift-drag ratios in the 80- to 100-knot (135 to 169 fps) speed range equal to or greater than those obtained on thin supercavitating hydrofoils.

INTRODUCTION

A hydrofoil designed for efficient operation at speeds of around 100 knots (169 fps) and depths of submersion of 5 feet or less will usually be very thin. If the hydrofoil section is designed to operate fully wetted by using conventional airfoil-thickness distributions, it must be thin in order to avoid cavitation on the upper surface. If a supercavitating hydrofoil (such as discussed in refs. 1, 2, and 3) is considered, the section must be thin (particularly near the leading edge) in order to obtain optimum values of lift-drag ratios. Thin sections, of course, present considerable structural problems.

The present investigation concerns an attempt to obtain acceptable hydrodynamic efficiency in the 100-knot speed range with relatively thick, structurally desirable sections. Principles of both fully wetted and supercavitating flow theory are utilized in the design of a hydrofoil with mean-line camber having a parabolic thickness distribution. This paper describes the principles involved in the design of such a section and the results of a preliminary experimental investigation of a cambered parabola with an aspect ratio of 1.

SYMBOLS

A	aspect ratio, b^2/S
a	fraction of chord from leading edge over which design load is uniform
b	hydrofoil span, in.
c	chord, in.
$c_{l,d}$	two-dimensional design lift coefficient
C_D	drag coefficient, $\frac{D}{\frac{1}{2}\rho V^2 S}$
C_L	lift coefficient, $\frac{L}{\frac{1}{2}\rho V^2 S}$
$C_{L,d}$	three-dimensional design lift coefficient
C_m	pitching-moment coefficient about the leading edge, $\frac{M}{\frac{1}{2}\rho V^2 cS}$
$C_{p,min}$	minimum pressure coefficient, $\frac{p_{min} - p_o}{\frac{1}{2}\rho V^2}$
D	drag force, lb
E	Jones' edge correction factor, ratio of plan-form semiperimeter to span
L	lift force, lb
M	pitching moment about the leading edge, ft-lb
p_o	pressure at mean depth of hydrofoil, lb/sq ft
p_{min}	minimum local pressure, lb/sq ft

p_v water-vapor pressure, lb/sq ft

S hydrofoil area, sq ft

t base thickness of parabolic section

V speed, fps and knots

X,Y coordinate axes

x distance from leading edge along X-axis of hydrofoil, in.

$x_{c.p.}$ distance from leading edge along X-axis of hydrofoil to the center of pressure, ft

x_s distance from leading edge along X-axis of strut, in.

y_l distance from X-axis to point on the lower surface of hydrofoil, in.

y_s distance from X-axis to point on surface of strut, in.

y_u distance from X-axis to point on upper surface of hydrofoil, in.

α hydrofoil angle of attack, measured from X-axis of section, radians unless otherwise specified

α_i induced angle of attack, radians unless otherwise specified

ρ mass density of water, $\frac{\text{lb-sec}^2}{\text{ft}^4}$

σ cavitation number, $\frac{p_o - p_v}{\frac{1}{2}\rho V^2}$

σ_i cavitation number at inception, $\frac{p_o - p_v}{\frac{1}{2}\rho V^2} = -C_{p,min}$

τ plan-form correction factor

DESIGN PRINCIPLES

The design of a hydrofoil for fully wetted operation at high speeds requires careful consideration of the minimum pressure coefficients that will be sustained on the hydrofoil. This pressure coefficient is defined as

$$C_{p,min} = \frac{p_{min} - p_o}{\frac{1}{2}\rho V^2} \tag{1}$$

where p_{min} is the minimum pressure on the hydrofoil, p_o is the free-stream pressure, ρ is the mass density of the fluid, and V is the free-stream velocity. If the fluid is water, p_{min} is limited to the vapor pressure of the water. When this limit is reached, the water changes from a fluid to a vapor and no further reduction of pressure is possible. Vapor cavities form on the hydrofoil in regions in which the local pressure has been reduced to vapor pressure. Such flow is called cavitation or cavity flow. The pressure coefficient is then

$$C_p = \frac{p_v - p_o}{\frac{1}{2}\rho V^2} \tag{2}$$

where p_v is the vapor pressure of the water. The dimensionless number, designated cavitation number, which defines such cavity flow is the negative of this pressure coefficient. That is,

$$\sigma = \frac{p_o - p_v}{\frac{1}{2}\rho V^2} = -C_p \tag{3}$$

For constant values of p_v and ρ, the cavitation number defines the relation between p_o and V that will produce cavitation. That is, for a given p_o, the speed at which a hydrofoil with a given C_p will cavitate is defined. Cavitation will first occur on the hydrofoil

where C_p is a minimum. This is designated the incipient cavitation number or

$$\sigma_i = -C_{p,min}$$

and defines the combination of p_o and V at which cavitation is incipient. If p_o is decreased or V is increased from these values, σ will become less than σ_i. As the local pressures which had been initially greater than p_{min} are reduced to p_v, the extent of cavitation on the hydrofoil increases. A value of σ greater than σ_i indicates that p_{min} is greater than p_v, and cavitation does not occur. The severity of cavitation accordingly increases as $\sigma_i - \sigma$ increases.

An ideal hydrofoil designed for operation at a particular value of σ should have a constant chordwise pressure coefficient on the upper surface as close to $-\sigma$ as feasible to obtain the maximum possible lift without causing cavitation. Such a pressure distribution is readily obtained on a thin lamina by using the proper camber, that is, the $a = 1.0$ mean line given in reference 4. However, to be of any use, some thickness is required for structural reasons. The thickness distribution used should be chosen to give as nearly a uniform pressure reduction due to thickness as possible.

A two-dimensional, elliptical thickness distribution produces fairly uniform pressure reductions over the chord and, for thin sections, has a minimum pressure coefficient approximately equal to twice the thickness-chord ratio. An indication of the thickness of a hydrofoil with an elliptic thickness distribution can be obtained from the following example: For a hydrofoil cambered with an $a = 1$ mean line for a design lift coefficient of 0.1, pressure coefficients of -0.05 and 0.05 will be obtained on the upper and lower surface, respectively. For a speed of 100 knots (169 fps) and a depth of submersion of 5 feet or less, a minimum pressure coefficient of about -0.08 is permissible without cavitation. Since the thickness contributes to the pressure distribution but not to the lift, a pressure-coefficient margin of 0.03 is available for the thickness. The elliptical thickness distribution which will produce a further reduction in the pressure coefficient of only 0.03 can have a thickness ratio of only 0.015. A 1.5-percent-thick hydrofoil, however, is not structurally adequate.

Another approach to the thickness problem is the use of an open thickness distribution such as a wedge or a parabola rather than a closed one such as an ellipse. An open thickness distribution results in a hydrofoil with a blunt base. Consequently, at relatively low speeds, a vapor cavity resulting in a base drag equal to the product of the base area and the vapor pressure will form at the base. In hydrodynamic flows

near the free surface it is possible to reduce this base drag by admitting air at atmospheric pressure to the base of the hydrofoil. Such a process is called ventilation and results in an air-filled cavity at the base of the hydrofoil. When the hydrofoil is operated at shallow depths of submersion, the pressure in the vented cavity is almost equal to the pressure at the mean depth of the hydrofoil p_o and thus the cavitation number based on the cavity pressure is nearly zero. The base drag for this condition is also essentially zero, and the profile drag of the section then depends only on the integral of pressures over the forebody. It has been shown in reference 5 that the forebody shape which produces the minimum drag for a noncambered section at zero angle of attack is a parabola. For parabolic sections of moderate base-thickness-to-chord ratio, it is shown in reference 5 that the profile drag coefficient at zero cavitation number is $\frac{\pi}{8}\frac{t}{c}$ and that the pressure coefficient is almost uniformly zero over most of the chord.

Thus, by using a parabolic thickness distribution instead of a conventional airfoil section with a sharp trailing edge, a two-dimensional hydrofoil section can be designed with a relatively thick section but without the thickness contributing to the minimum pressure coefficient of the section. Such a section does have a larger profile drag than a fully wetted section with a closed thickness distribution but by using a parabolic open-type thickness distribution with the blunt base vented to the atmosphere, the profile drag may be minimized. A possible method of achieving ventilation of the hydrofoil base is to support the hydrofoil with a surface-piercing blunt-based strut so that air may pass down the rear of the strut to the hydrofoil base. To minimize the strut drag, the strut should also have a parabolic cross section.

The purpose of the present investigation was to design a low-aspect-ratio, cambered-parabolic hydrofoil for a speed of about 100 knots (169 fps) and to determine experimentally its hydrodynamic characteristics over a range of speeds and angles of attack.

DESCRIPTION OF MODEL

The cambered-parabolic model designed for experimental investigation is shown in figure 1. An aspect ratio of 1 was chosen for the model in order to compare the experimental results with those obtained on the supercavitating hydrofoils with aspect ratios of 1 investigated in reference 2. The chord of the model was 7.071 inches, and the total hydrofoil area was 50 square inches. The base-thickness-to-chord ratio of the parabolic thickness distribution selected was 0.1. This thickness was considerably more than was required for strength but was chosen because the purpose of the investigation was to study a thick, high-speed hydrofoil.

Since the hydrofoil aspect ratio of one is so small and the hydrofoil operates near the free water surface, the exact shape required to produce a uniform pressure over the upper surface is difficult to determine. The desired uniform pressure coefficient over the upper surface was chosen to be 0.07, corresponding to a three-dimensional design lift coefficient of 0.14.

By neglecting cross-flow and free-water-surface effects the lift coefficient of a finite span, fully wetted airfoil or hydrofoil is given by Jones in reference 6 and may be written as

$$C_L = \frac{1}{E}\left[c_{l,d} + 2\pi(\alpha - \alpha_i)\right] \tag{4}$$

where

C_L lift coefficient at finite aspect ratio

E ratio of plan-form semiperimeter to span and is $\frac{A + 1}{A}$ for rectangular plan forms where A is the aspect ratio

$c_{l,d}$ two-dimensional lift coefficient produced by the camber of the section

α geometric angle of attack, defined as $\alpha = 0$ when total two-dimensional lift coefficient is $c_{l,d}$

α_i induced angle of attack, $(1 + \tau)\frac{C_L}{\pi A}$ where τ is a correction for plan form (see ref. 7)

The induced angle of attack α_i is uniform over the span for an elliptic spanwise loading. However, in the case of rectangular plan forms, the induced angle as given in equation (4) is only an average value. The actual induced angle is less than the average at the center of the span and greater at the tips. Also, it is not exactly true that the induced angle is a true angle-of-attack-type contribution to the chordwise pressure distribution; that is, some of the reduction in lift attributed to α_i actually is caused by a change in the camber-type pressure distribution. If these two effects are neglected and α_i is assumed to be a true uniform spanwise change in angle of attack, then in the three-dimensional case when $\alpha = \alpha_i$, all the lift will be produced by the camber. For this condition, equation (4) may be written as

$$C_{L,d} = \frac{1}{E} c_{l,d} = \frac{A}{A + 1} c_{l,d} \qquad (5)$$

Since a three-dimensional design lift coefficient of 0.14 was prescribed for the model with an aspect ratio of 1, equation (5) shows that the camber required to produce this value must correspond to a two-dimensional lift coefficient of 0.28. Therefore, the mean line of the model was uniformly cambered in accordance with the $a = 1.0$ mean line of reference 4 for a two-dimensional design lift coefficient of 0.28.

The model was supported by a parabolic strut with a 4.0-inch chord and a base-thickness-to-chord ratio of 0.15. The strut is also shown in figure 1. The model and strut were both made of stainless-steel polished to a smooth finish. The intersection between model and strut was without fillets.

APPARATUS AND PROCEDURE

Facility

Since the speed of primary interest in the investigation was around 170 fps, the model was tested in the Langley high-speed hydrodynamics facility described in reference 8. However, the carriage used in the investigation is a new one which is lighter than that described in reference 8. The new carriage, shown in figure 2, is capable of speeds up to 250 fps. The maximum speed used in the present investigation was about 190 fps. As described in reference 8, the carriage is accelerated by a water jet that is operated by compressed air and impinges on a turning bucket on the rear end of the carriage. The carriage then coasts freely during a 1,200-foot test run and is brought to a stop by a cable arresting system that engages the receiver on the front end of the carriage. For the present investigation the deceleration while coasting varied between 0.06g units and 0.2g units.

Balance

Lift, drag, and pitching moment were measured by an electrical strain-gage balance attached to a hydraulically operated staff on the end of the boom overhanging the tank (fig. 3). The forces were recorded on strip charts located in the instrument house.

The angle of attack of the model was measured from the X-axis of the section shown in figure 1. Changes in angle of attack of the model due to structural deflections were obtained during the calibration of

the balance, and the angles of attack measured during the investigation were corrected for this change. The change was approximately 0.1° or less for all angles and speeds investigated.

Pressures

A few pressures were measured during the investigation at the center of the base of the hydrofoil and at the base of the strut 2 inches above the center of the model. These orifices were connected to pressure cells whose outputs were recorded continuously during the testing by an oscillograph.

Photographs

Photographs were taken from above water, from the side underwater, and from the bottom underwater at selected stations along the tank. These photographs were used to study flow characteristics. A magnetic device was employed to indicate on the balance record when the photographs were taken and thus to provide synchronization between the photographs and the force data. The associated speed was determined by electronically measuring the time for the model to travel a distance of 10 feet across the photographic station.

Accuracy and Scope

The accuracy of the quantities measured is estimated to be within the following limits:

Lift coefficient	0.001
Drag coefficient	0.0002
Pitching-moment coefficient	0.0004
Angle of attack, deg	±0.1
Speed, fps	±0.15

The density of the tank water used in computing the force coefficients was 1.94 slugs/cu ft. The kinematic viscosity during the test was 1.42×10^{-5} sq ft/sec.

The depth of submersion of the leading edge of the model was set at 3.5 inches at the beginning of each test. This depth corresponds to a depth-chord ratio of 0.5. The model was investigated over a range of angles of attack between 1° and 8° and a speed range of 130 to 190 fps.

RESULTS AND DISCUSSION

The data obtained are presented in figure 4 as plots of speed with angle of attack as the parameter against lift coefficient, drag coefficient, pitching-moment coefficient about the leading edge, distance from the center of pressure to the leading edge in chords, and lift-drag ratio. The drag data presented in figure 4 are based on the total measured drag reduced by a calculated drag for the strut. The calculated strut drag included the skin friction of both sides of the strut, the profile drag of the strut at zero cavitation number obtained from reference 5, and the base drag of the strut as determined from an integration of the measured pressures. An estimate of the aerodynamic tares of that portion of the strut above the water surface indicated these tares to be negligible.

The measured pressures reveal that complete ventilation of the strut and hydrofoil bases did not occur. Motion pictures of the flow near the strut—water-surface intersection showed that the film of water which "rides" up the strut closes behind the strut in a very short distance; thus the air passageway is partially closed. The average pressures measured over the bases of the strut and hydrofoil were about 1,500 lb/sq ft and 600 lb/sq ft abs, respectively. The drag associated with this incomplete ventilation amounts to from 20 to 30 percent of the total drag. It would be desirable, therefore, to find a means to ventilate the bases more completely to reduce the drag. No effort to open the strut cavity at the surface was made in the present investigation.

No cavitation was observed on the upper surface of the model at an angle of attack of 1° for the range of speeds investigated. However, photographs of the model at an angle of attack of 1° revealed that cavitation was incipient on the lower surface of the model starting at the leading edge at a speed of about 130 fps. This lower surface cavitation combined with the total positive lift recorded indicates that the net lift over the forward portion of the section was negative while that over the rearward portion was positive. Such a chordwise loading explains the unusually far rearward location of the center of pressure obtained for an angle of attack of 1° in figure 4(e).

No cavitation was observed on the lower surface at an angle of attack of 2°. However, traces of cavitation did appear all over the upper surface at speeds in excess of about 152 fps. At an angle of attack of 2.5°, cavitation was incipient on the center portion of the upper surface near the leading edge at a speed of about 130 fps. This cavitation zone increased in length with increase in speed until at the maximum speed tested of 182 fps, the cavity covered about 75 percent of the chord in the central portion of the span. The cavity on the outboard 25 percent of the span varied almost linearly in length from zero at the tip to about 75 percent of the chord at a point 0.25 chord inboard of the tip.

The discontinuity which appears in figure 4 for an angle of attack of 3° at 157 fps and for 3.5° at 139 fps is caused by sudden ventilation of portions of the upper surface. Figure 5(a) shows a photograph of the flow on the upper surface of the hydrofoil for an angle of attack of 3.5° and a speed of 132 fps. This photograph shows cavitation extending from the leading edge to a point about 40 percent of the chord downstream. Figure 5(b) shows this same condition at a speed of 144 fps. Evidently, cavitation progressed downstream as the speed increased until at a speed less than 144 fps, the vapor cavity intercepted the vented flow and caused ventilation of the portion of the span shown in figure 5(b). This venting results in an abrupt change in the forces on the model.

Figure 6(a) is a photograph of the upper surface of the model at an angle of attack of 4° and a speed of 155 fps. It may be seen that a vented cavity exists on the entire upper surface of the model for this condition. Figure 6(a) is also representative of the flow at speeds as low as 130 fps for this angle of attack of 4°. Figure 6(b) shows a view of the upper surface of the hydrofoil at an angle of attack of 8° and a speed of 158 fps. The vented flow shown in figure 6(b) is representative of all conditions tested for angles of attack greater than 4°.

Lift coefficient and lift-drag ratio plotted against angle of attack and lift-drag ratio plotted against lift coefficient are presented in figure 7. These curves were obtained by cross plotting from figure 4 for constant speeds of 80, 90, and 100 knots (135, 152, and 169 fps). Figure 7(a) shows the influence on the lift coefficient of the spread of cavitation discussed in connection with figures 4, 5, and 6. At a speed of 80 knots, an angle of attack of 3.5° was attained before cavitation resulted in a break in the lift-curve slope. At the higher speeds of 90 and 100 knots, the breaks occurred at angles of attack of 3° and 2.5°, respectively. Above these angles of attack, the lift-curve slope decreased rapidly and actually reversed at the speeds of 80 and 90 knots as the extent of cavitation increased. At an angle of attack of about 5°, the hydrofoil was supercavitating at all three speeds and the lift-curve slope increased and was identical for all three speeds.

Before discussing figure 7 further it is important to note that although the design angle of attack in the two-dimensional case would be zero, the design angle must be modified in the three-dimensional case because of the induced angle of attack. For example, if the water-surface proximity is neglected, the induced angle for a lift coefficient of 0.14 is roughly $\frac{(0.14)^2}{\pi A}$ radians or about 2.5° for an aspect ratio of one. The influence of the free surface further increases this value; therefore, the design angle of attack of the present model must be about 3°. This value of 3° is, of course, only a nominal value. The actual induced angle is less at the center of the span and greater at the tip

as pointed out in the section describing the model design. Therefore, it is not possible to prescribe a design angle of attack in terms of an angle of attack for which all the lift is due to camber. The design angle of attack must now be defined in terms of the angle of attack which produces the greatest lift-drag ratio for a given speed. In this sense, figure 7(b) shows that the optimum angle of attack is 3.5° at 80 knots, 3.0° at 90 knots, and about 2.5° at 100 knots. It should be possible to improve the performance of this type section by a more detailed design incorporating the proper spanwise distribution of camber and angle of attack; however, the more sophisticated design should be of less importance at higher aspect ratios. The characteristics of the cambered parabola are compared in figure 8 with experimental data obtained at high speeds on the flat-bottomed and the cambered, aspect-ratio-one supercavitating sections described in reference 2. The data presented for these supercavitating sections were obtained in the Langley high-speed hydrodynamics facility at a depth-chord ratio of 0.5. The characteristics of the supercavitating sections were found to be essentially constant over the 80- to 100-knot speed range. The cambered-parabola data are taken from figure 7(c) for speeds of 80 and 100 knots. Figure 8 shows that at 80 knots the cambered-parabolic section has a higher lift-drag ratio than either the flat or cambered supercavitating section and at 100 knots it has about the same maximum lift-drag ratio as the flat plate. The low maximum lift-drag ratio of the cambered supercavitating section is due to the large amount of camber. A previous analysis has shown that a supercavitating section with only a small amount of camber would theoretically give a slightly higher lift-drag ratio than the flat plate. The important point to note is that in the speed range of 80 to 100 knots, the cambered parabola has a maximum lift-drag ratio about equal to and in some conditions higher than the maximum lift-drag ratio obtainable with supercavitating hydrofoils and the cambered parabola is much thicker. Thickness is particularly important since severe leading-edge vibrations were observed on the flat-plate section at speeds of 80 knots and higher.

L
6
5
4

CONCLUDING REMARKS

The cambered hydrofoil with an aspect ratio of 1 designed with a parabolic thickness distribution has a fairly narrow range of angle of attack for optimum efficiency. The lift, drag, and pitching-moment characteristics have discontinuities caused by the transition from a wetted to a vented upper surface as angle of attack or speed is increased. However, cambered parabolas provide a means of obtaining lift-drag ratios

in the 80- to 100-knot speed range equal to or greater than those obtained on supercavitating hydrofoils, and the cambered parabola can be thicker and stronger.

Langley Research Center,
National Aeronautics and Space Administration,
Langley Field, Va., July 28, 1959.

REFERENCES

1. Tulin, M. P., and Burkart, M. P.: Linearized Theory for Flows About Lifting Foils at Zero Cavitation Number. Rep. C-638, David W. Taylor Model Basin, Navy Dept., Feb. 1955.

2. Johnson, Virgil E., Jr.: Theoretical Determination of Low-Drag Supercavitating Hydrofoils and Their Two-Dimensional Characteristics At Zero Cavitation Number. NACA RM L57G11a, 1957.

3. Johnson, Virgil E., Jr.: Theoretical and Experimental Investigation of Arbitrary Aspect Ratio, Supercavitating Hydrofoils Operating Near the Free Water Surface. NACA RM L57I16, 1957.

4. Abbott, Ira H., Von Doenhoff, Albert E., and Stivers, Louis S., Jr.: Summary of Airfoil Data. NACA Rep. 824, 1945. (Formerly NACA WR L-560.)

5. Tulin, M. P.: Supercavitating Flow Past Foils and Struts. Cavitation in Hydrodynamics, NPL (Teddington, England), 1956, 16 p. 1 - 16 p. 19.

6. Jones, Robert T.: Correction of Lifting-Line Theory for the Effect of the Chord. NACA TN 817, 1941.

7. Glauert, H.: The Elements of Aerofoil and Airscrew Theory. Second ed., Cambridge Univ. Press, 1947. (Reprinted 1948.)

8. Christopher, Kenneth W.: Investigation of the Planing Lift of a Flat Plate At Speeds up to 170 Feet Per Second. NACA TN 3951, 1957.

Hydrofoil Coordinates		
x	y_u	y_l
.000	.000	.000
.035	.030	.020
.053	.038	.024
.088	.050	.029
.177	.074	.037
.354	.115	.052
.530	.139	.055
.707	.163	.061
1.061	.204	.070
1.414	.237	.079
1.768	.265	.088
2.121	.290	.097
2.475	.311	.107
2.828	.330	.118
3.182	.346	.129
3.536	.359	.141
3.889	.370	.154
4.243	.380	.168
4.596	.387	.183
4.950	.392	.200
5.303	.395	.218
5.657	.395	.237
6.010	.392	.259
6.394	.386	.284
6.717	.376	.313
7.071	.354	.354

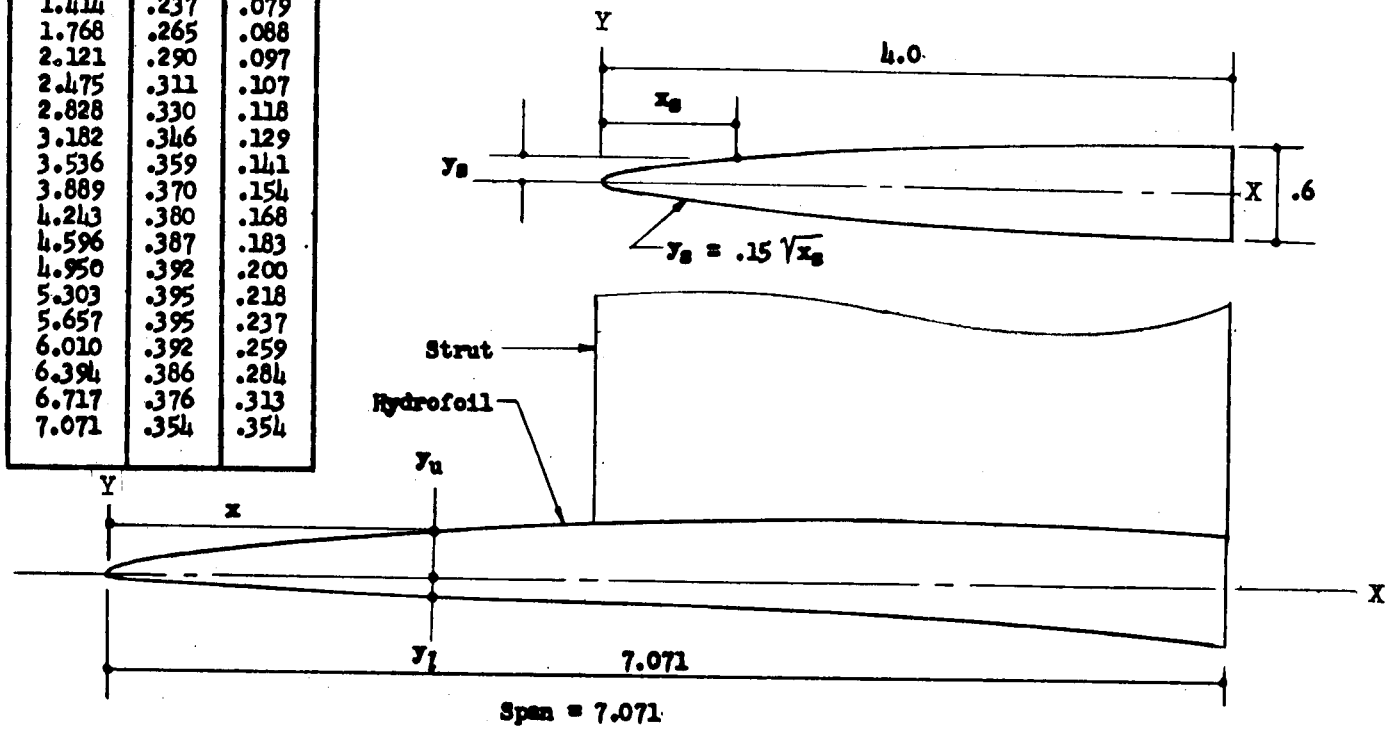

Figure 1.- Details of cambered-parabolic hydrofoil and supporting strut. All dimensions are in inches.

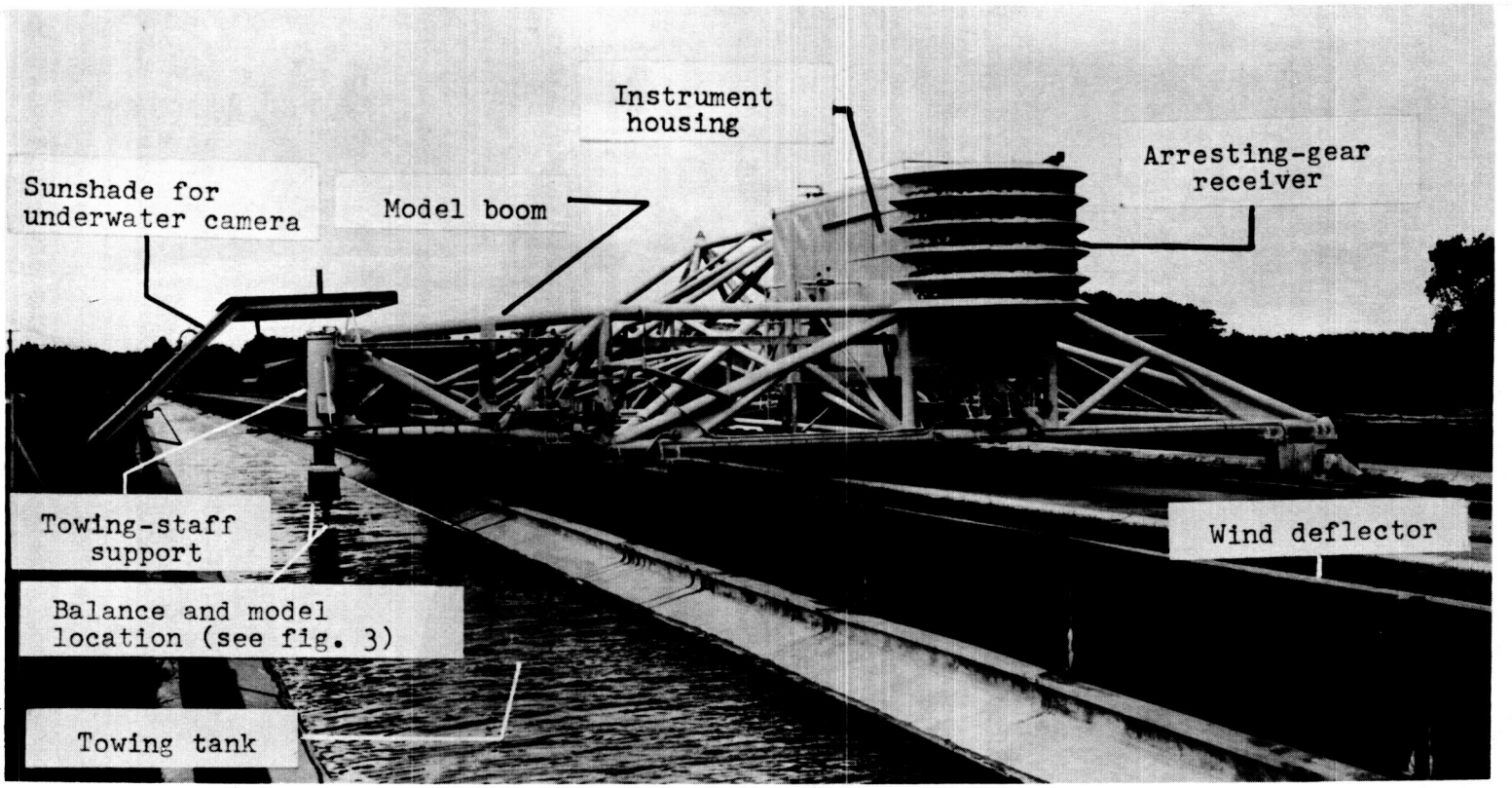

Figure 2.- Photograph of high-speed carriage. L-59-3840.1

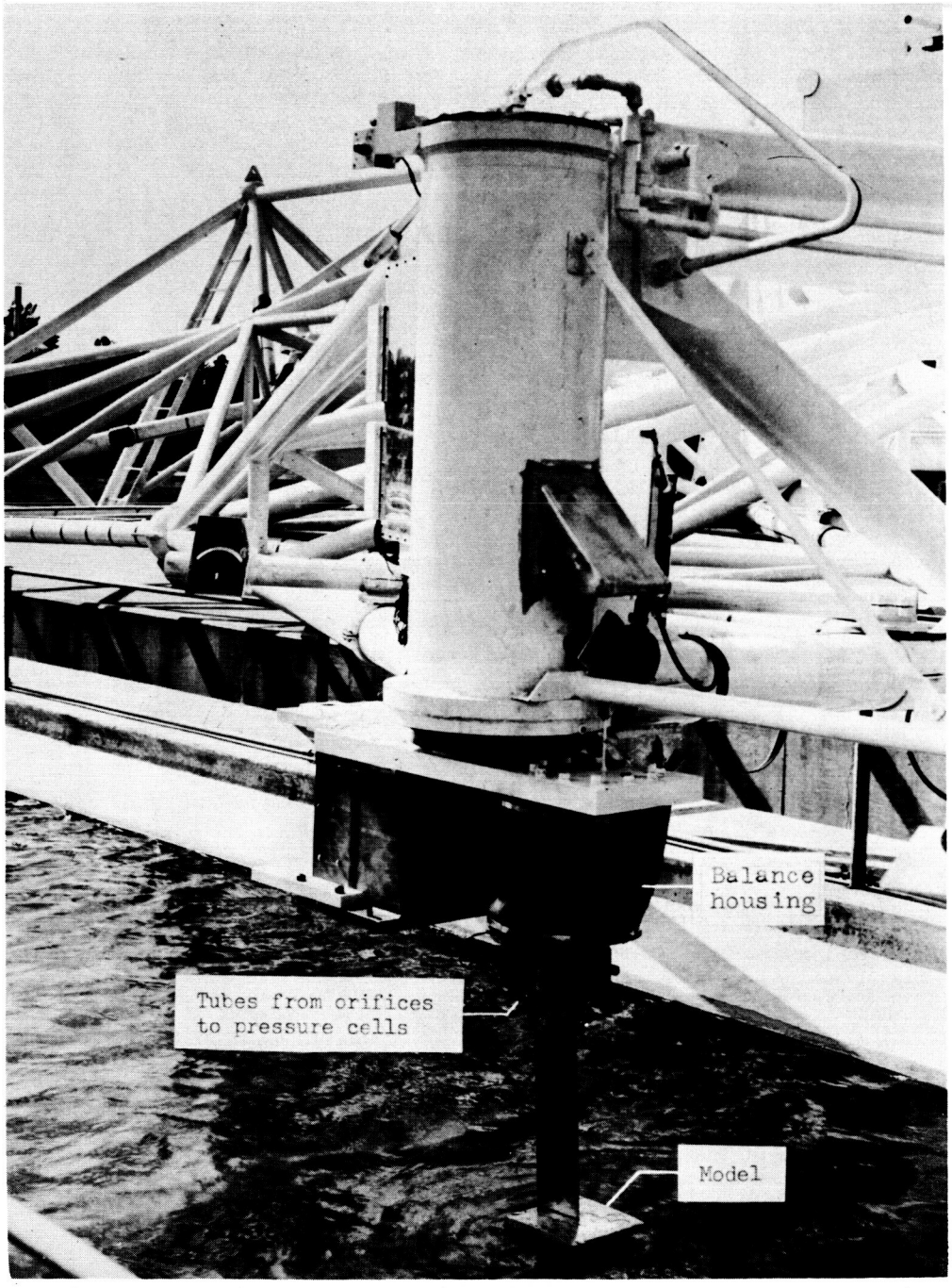

L-59-5013

Figure 3.- Photograph of test setup with cambered-parabolic hydrofoil installed.

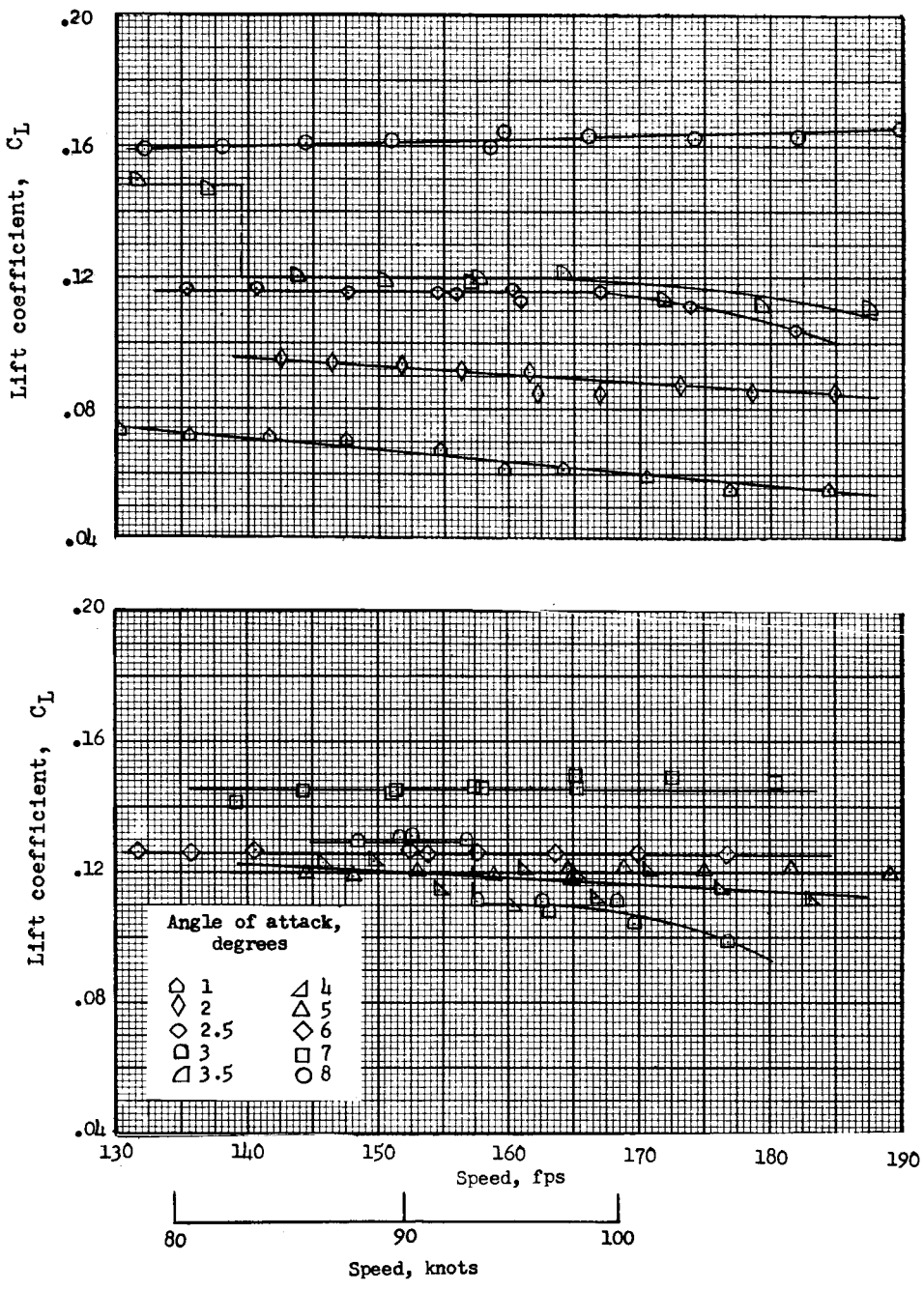

(a) Variation of lift coefficient with speed for angles of attack of 1°, 2°, 2.5°, 3°, 3.5°, 4°, 5°, 6°, 7°, and 8°.

Figure 4.- Hydrodynamic characteristics of cambered-parabolic hydrofoil.

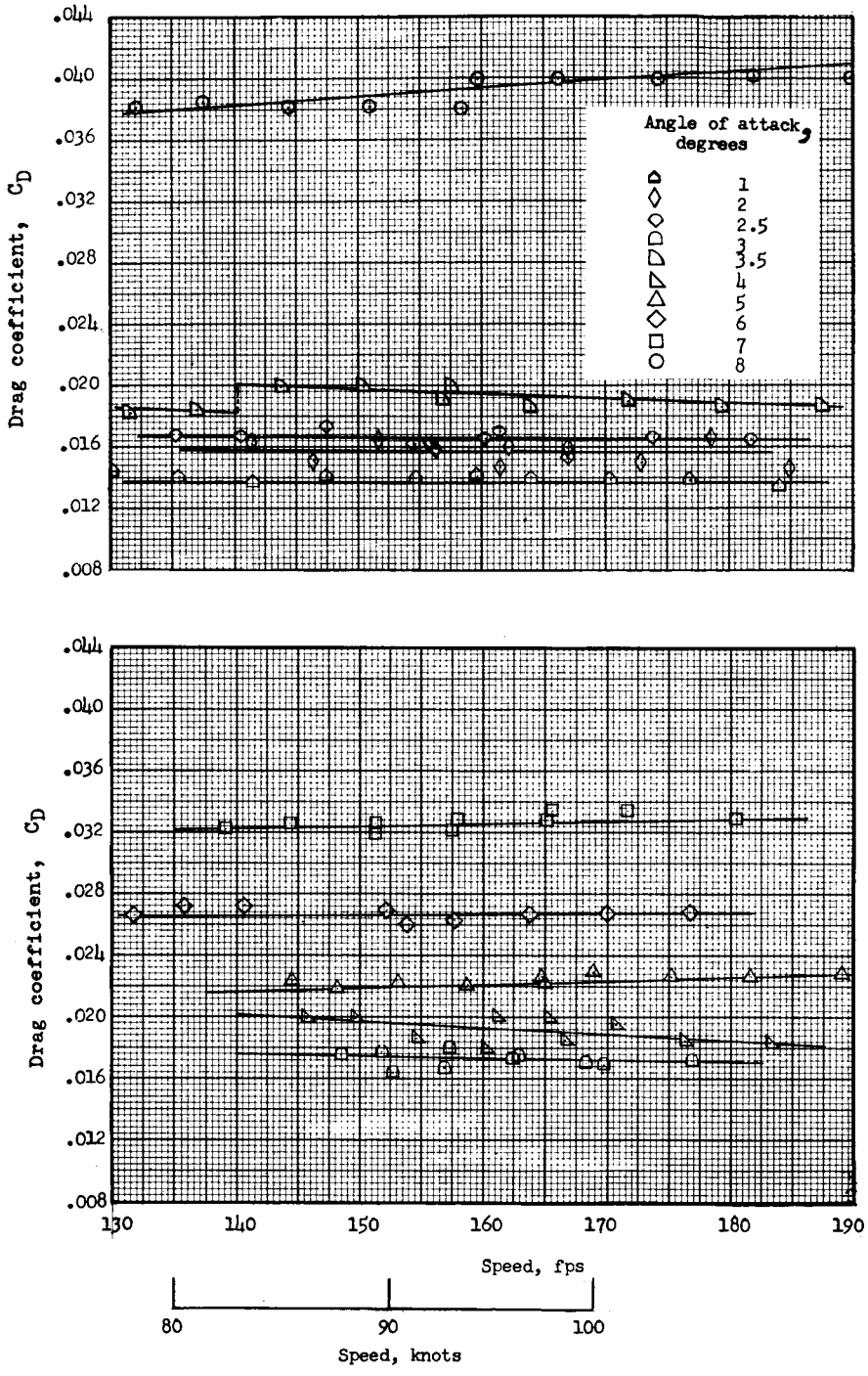

(b) Variation of drag coefficient with speed for angles of attack of 1°, 2°, 2.5°, 3°, 3.5°, 4°, 5°, 6°, 7°, and 8°.

Figure 4.- Continued.

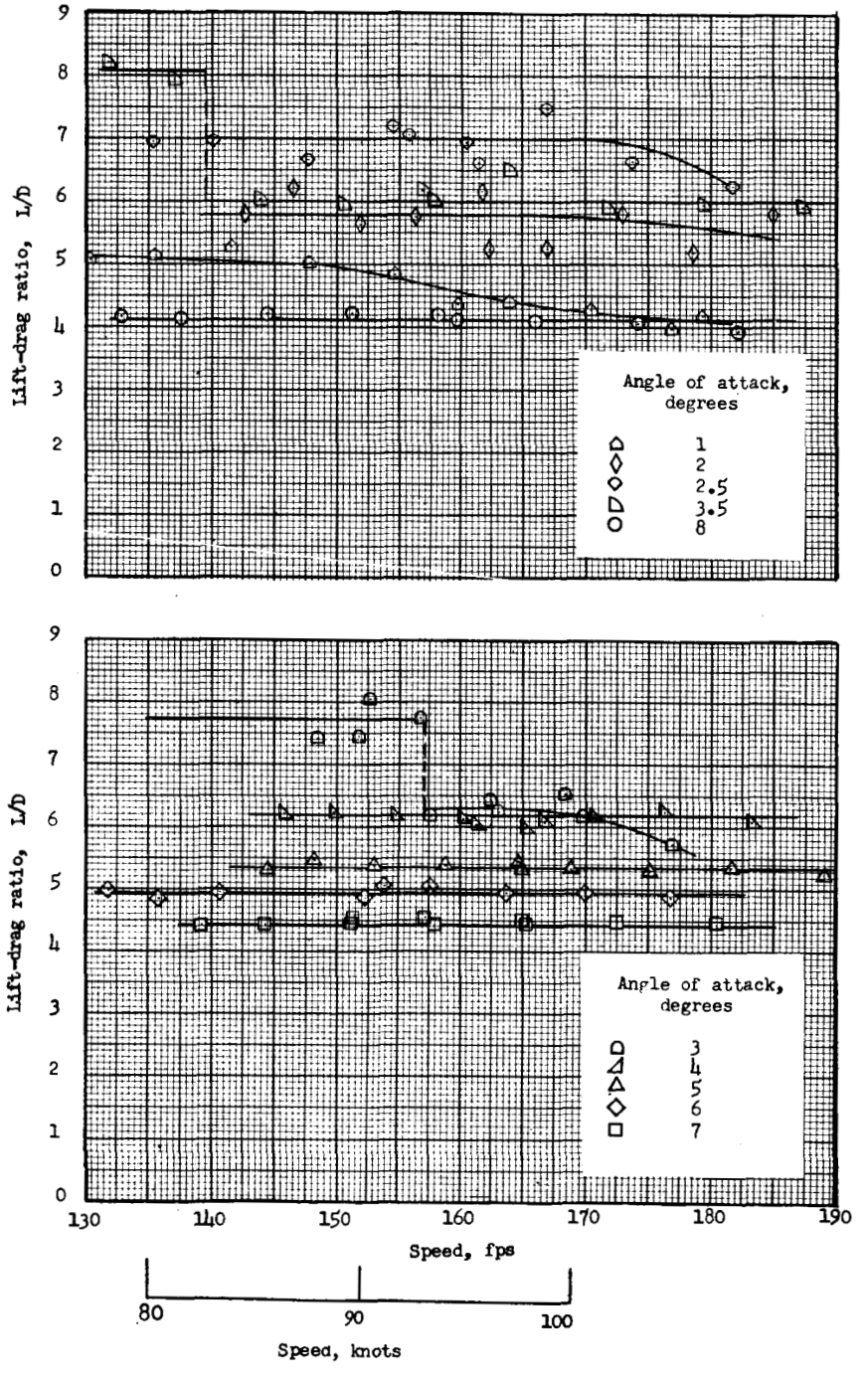

(c) Variation of lift-drag ratio with speed.

Figure 4.- Continued.

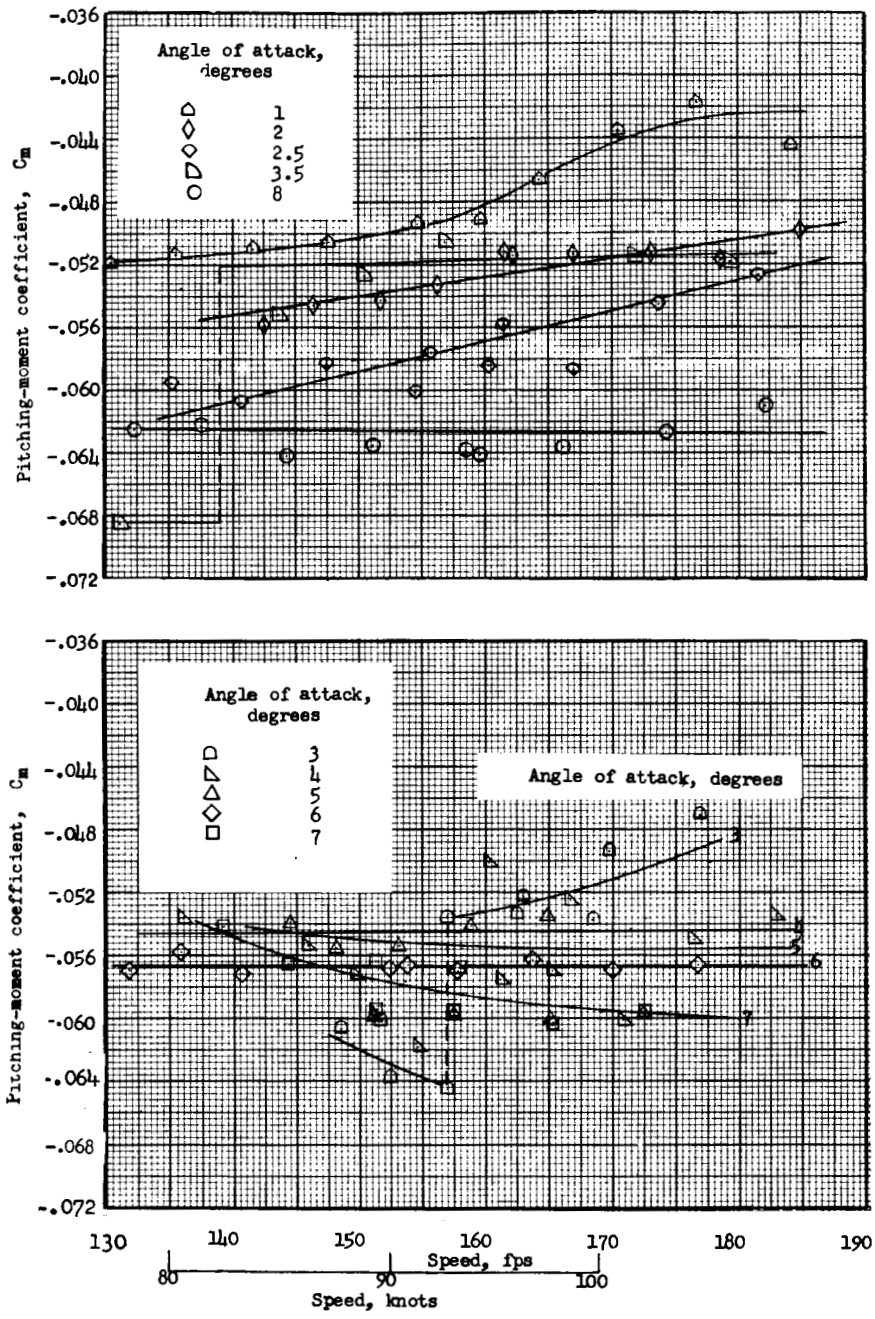

(d) Variation of pitching-moment coefficient about the leading edge with speed.

Figure 4.- Continued.

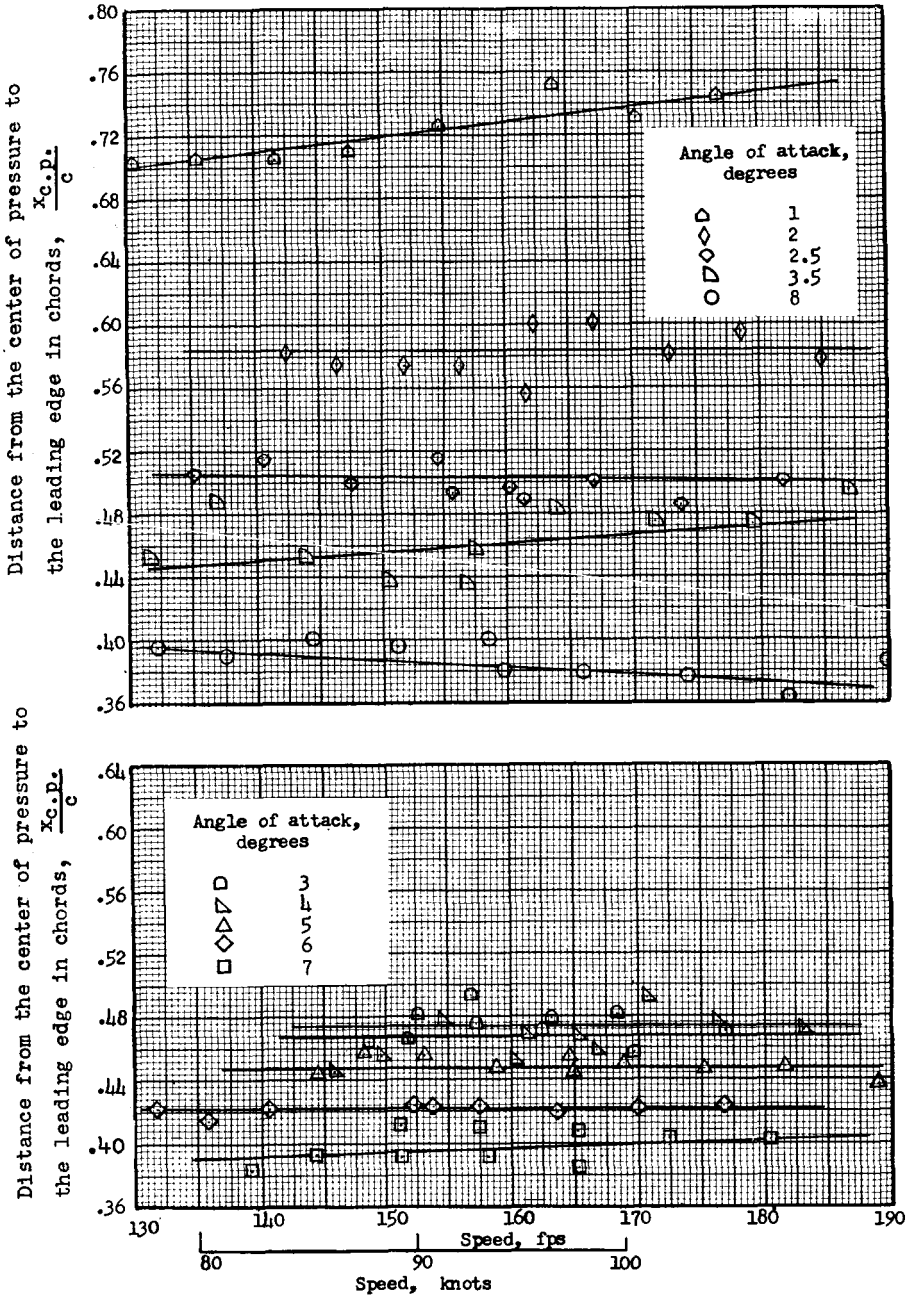

(e) Variation of the distance of the center of pressure from the leading edge in chords with speed.

Figure 4.- Concluded.

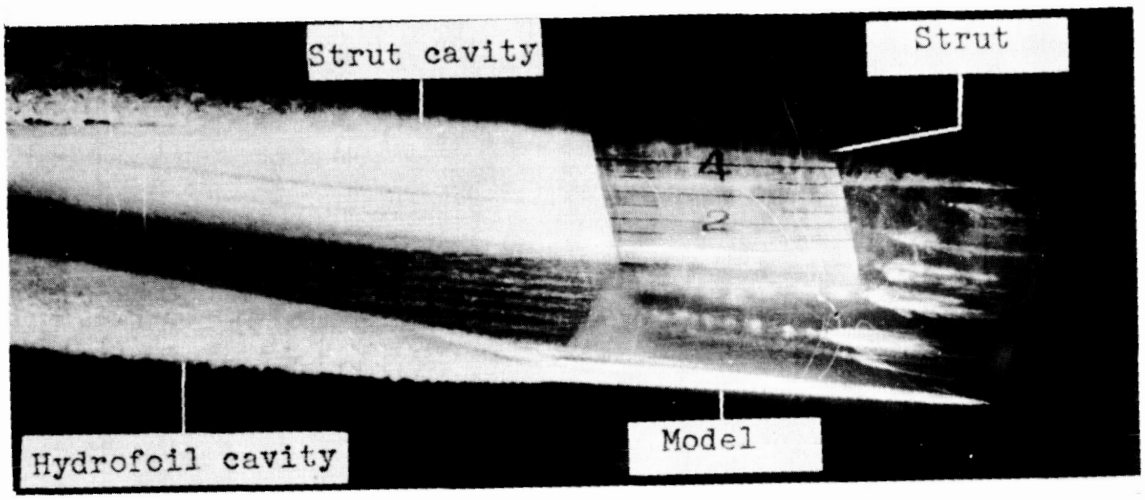

(a) Speed = 132 fps.

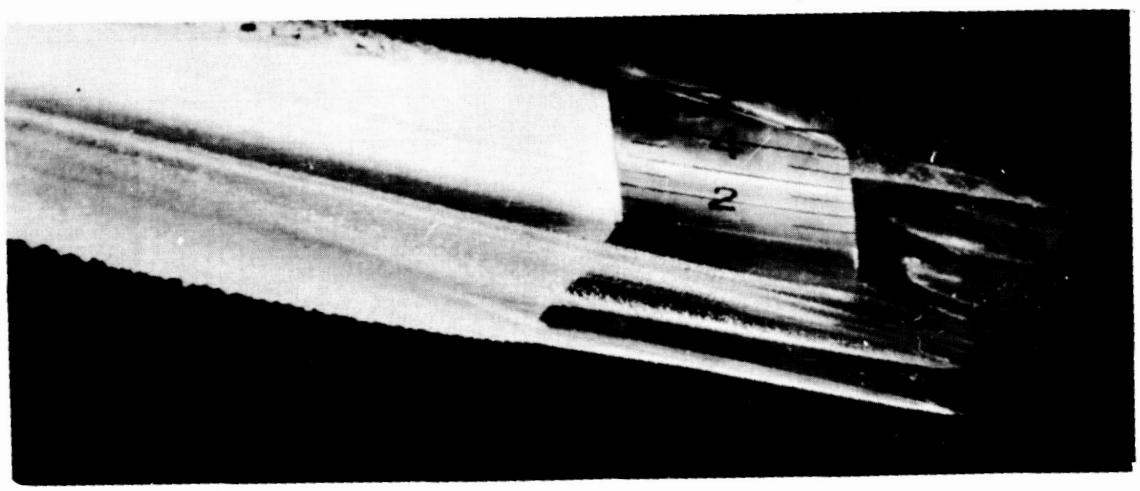

(b) Speed = 144 fps. L-59-5011

Figure 5.- Photographs of upper surface of cambered-parabolic hydrofoil operating at an angle of attack of 3.5°.

L-654

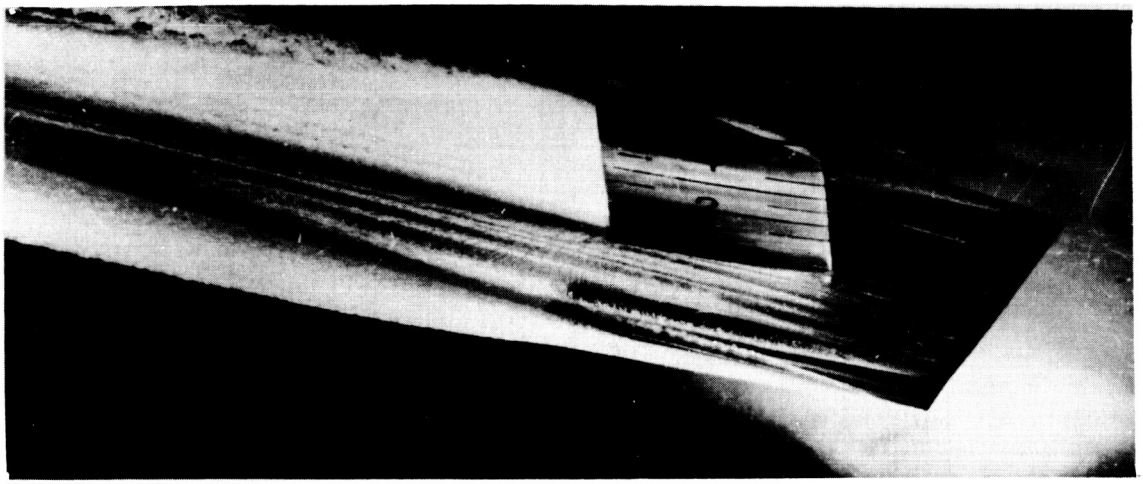

(a) Speed = 155 fps; angle of attack = 4°.

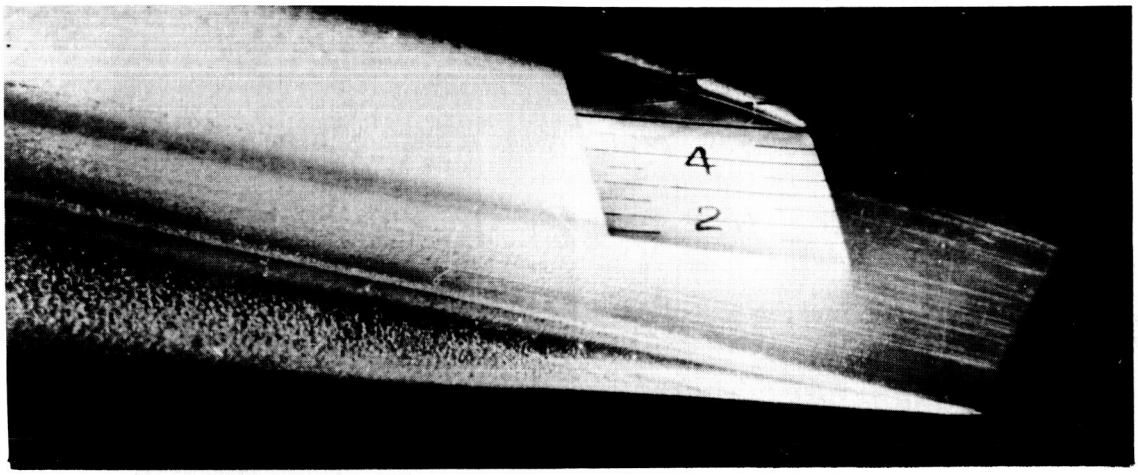

(b) Speed = 158 fps; angle of attack = 8°. L-59-5012

Figure 6.- Photographs of the upper surface of the cambered-parabolic hydrofoil with vented cavity from the leading edge.

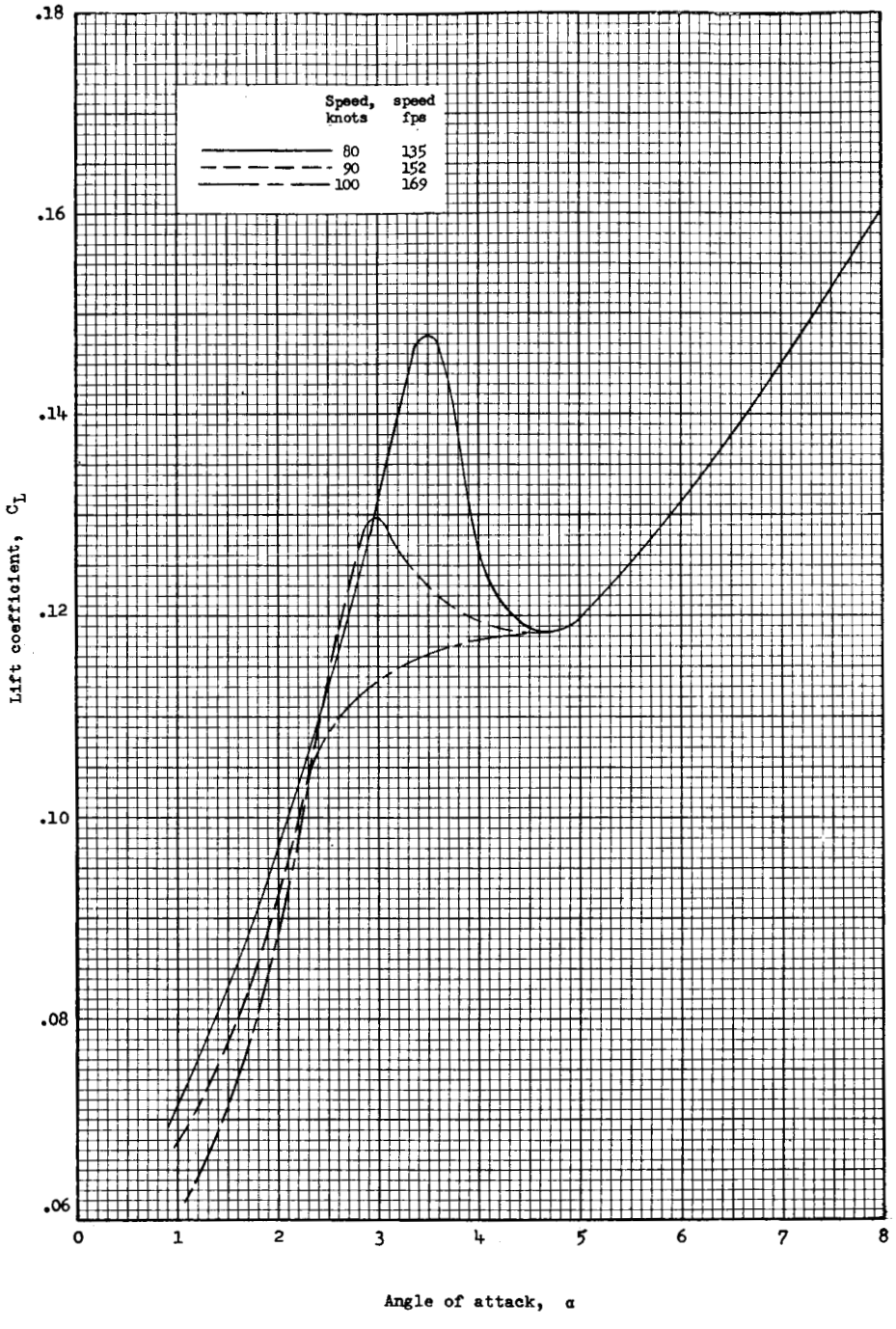

(a) Variation of lift coefficient with angle of attack.

Figure 7.- Hydrodynamic characteristics of the cambered parabola at constant speeds of 80, 90, and 100 knots.

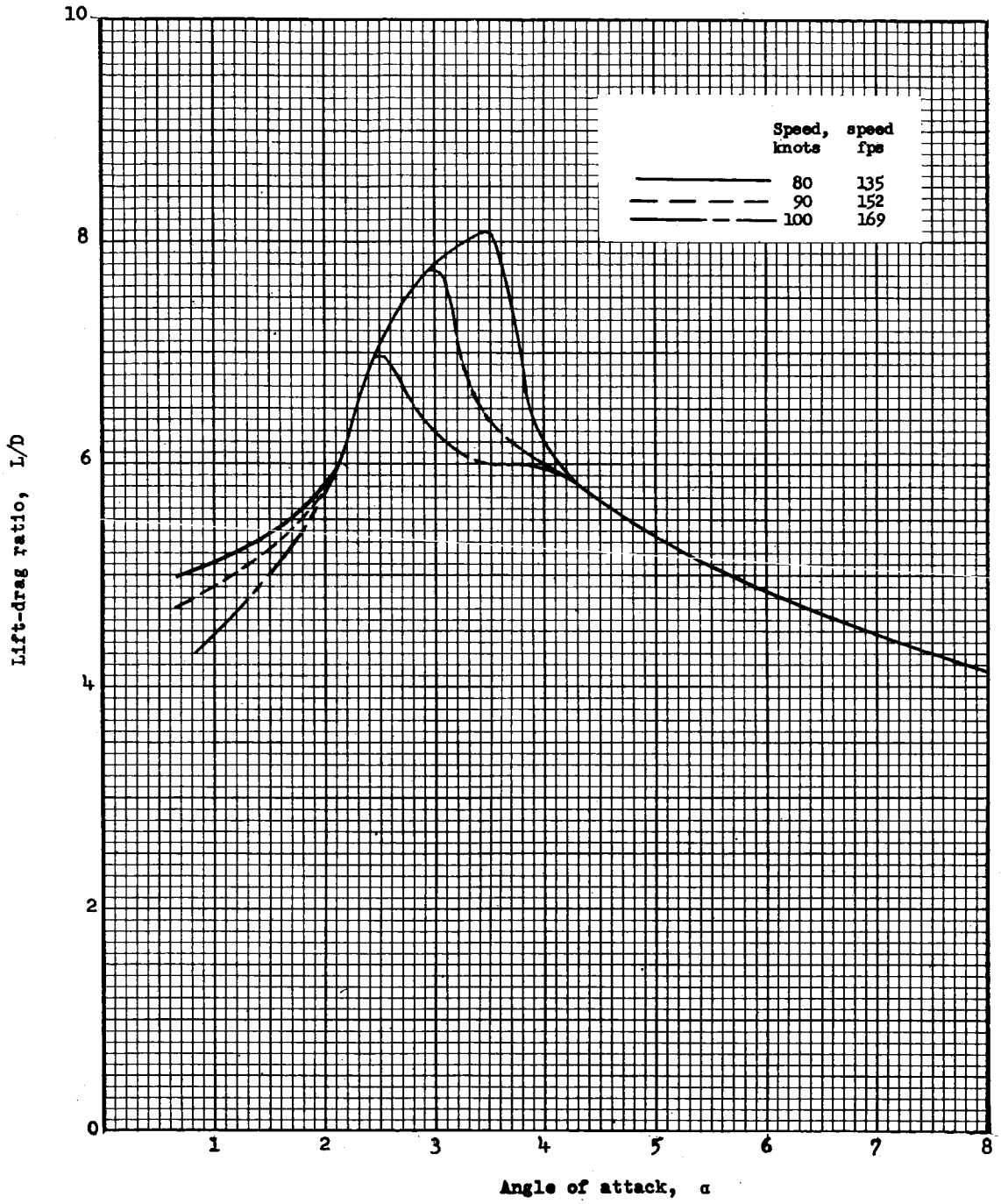

(b) Variation of lift-drag ratio with angle of attack.

Figure 7.- Continued.

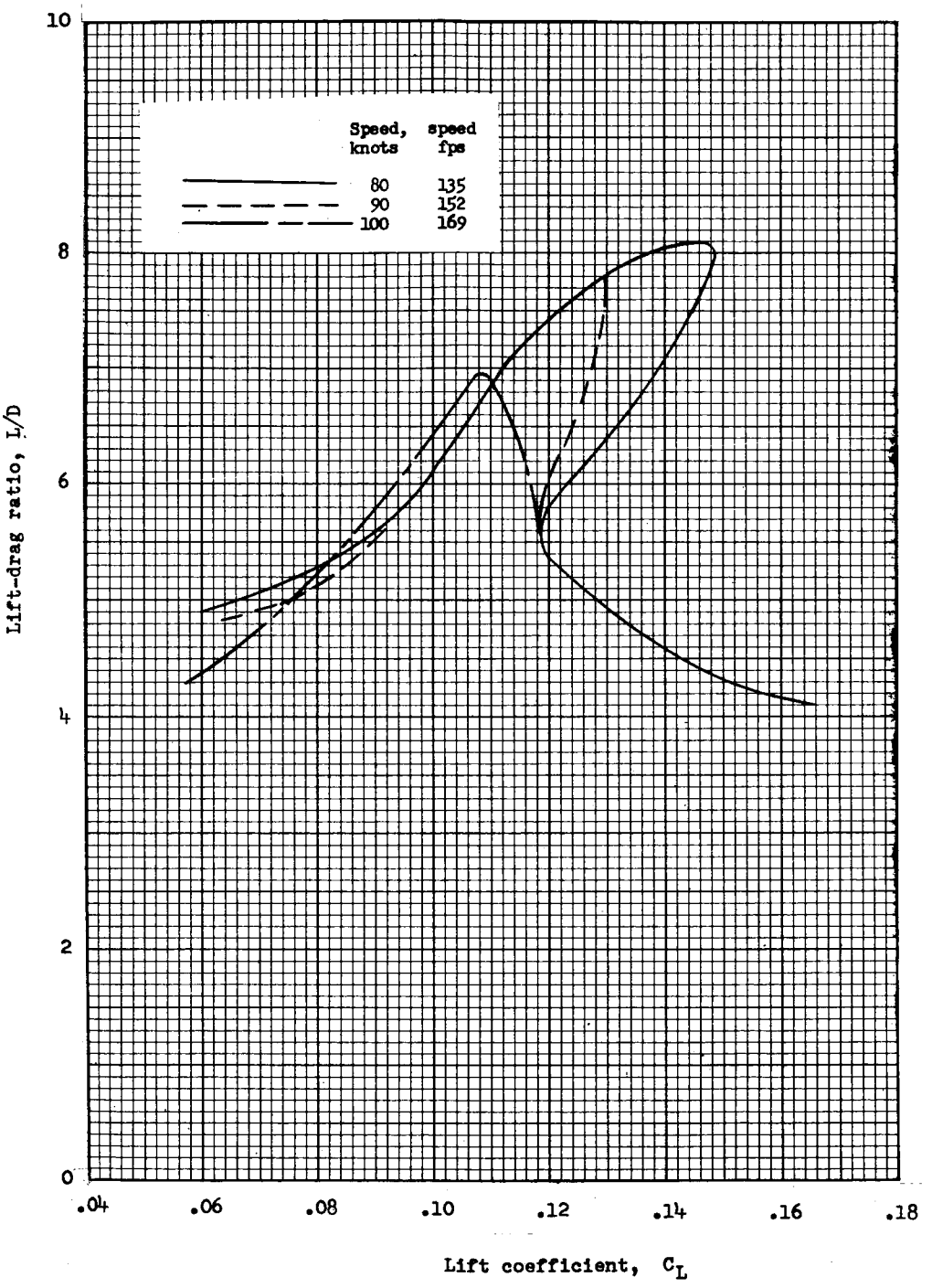

(c) Variation of lift-drag ratio with lift coefficient.

Figure 7.- Concluded.

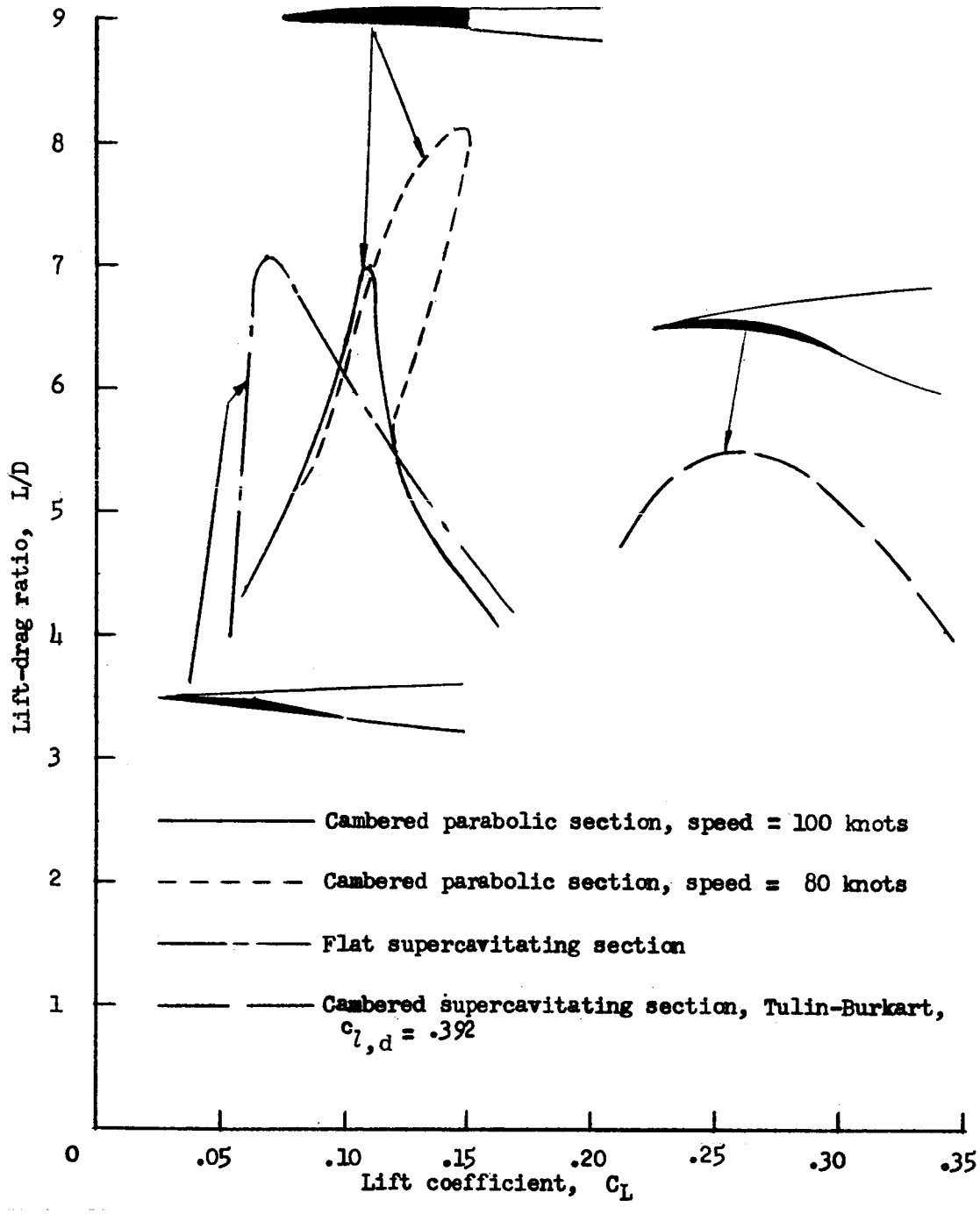

Figure 8.- Comparison of lift-drag ratios of cambered-parabolic section with lift-drag ratios of supercavitating sections. Aspect ratio = 1, depth-chord ratio = 0.5.